JOURNAL OF MATERIALS SCIENCE 26 (1991) 241–247

Effects of solute ion and grain size on superplasticity of ZrO_2 polycrystals

FUMIHIRO WAKAI
Ceramic Science Department, Government Industrial Research Institute, Nagoya, Hirate-cho, Kita-ku, Nagoya 462, Japan

TAKAYUKI NAGANO
Research and Development Centre, Suzuki Motor Co. Ltd, Hamamatsu 432-91, Japan

The deformation of ZrO_2 polycrystals containing 2 to 8 mol % Y_2O_3 or 12 mol % CeO_2 were investigated by uniaxial tension and tensile creep tests at elevated temperatures. It was found that there were two deformation mechanisms. The stress exponent was close to 2 for the fine-grained materials (less than 1 μm), but the exponent decreased with increasing grain size. This behaviour was analysed using a model based on grain-boundary sliding with diffusion accommodation, in which the diffusion creep controlled by interface-reaction and that controlled by diffusion of cations were incorporated. The diffusion coefficient of cations was greatly affected by the concentration of the solute ions. It was observed that there was a negative correlation between interface-reaction rate and Y_2O_3 concentration.

1. Introduction

Cubic ZrO_2 has the fluorite structure. When the crystal is doped with low valence cations such as Ca^{2+} or Y^{3+}, the diffusion rate of the anion becomes much greater than that of cations [1–5]. High anionic conductivity is also reported for tetragonal ZrO_2 [6, 7].

The deformation of polycrystalline materials at elevated temperatures is a phenomenon related to the ionic transport processes. The strain rate ($\dot{\varepsilon}$) is usually expressed by the following equation

$$\dot{\varepsilon} = A\sigma^n \exp\left(-\frac{Q_{app}}{RT}\right) \quad (1)$$

where σ is the stress, T is the absolute temperature, n is the stress exponent, Q_{app} is the apparent activation energy, R is the gas constant, and A is a coefficient. When the ambipolar coupling is incorporated, the diffusion creep of ionic polycrystals is controlled by the slower diffusing species; for ZrO_2 it is controlled by cations [8–12].

The Y_2O_3-stabilized tetragonal ZrO_2 polycrystals (Y-TZP) are superplastic and the deformation is characterized by a stress exponent of 2 [13]. The microstructural observation of deformed specimens, dislocation-free grains and equiaxed grain shape, suggested the major role of grain-boundary sliding (GBS) in the deformation mechanism [14–18].

Ashby and Verral [19] developed a model of superplasticity which involved GBS accommodated by diffusion. By considering the grain-switching events, they obtained the following equation for the strain rate ($\dot{\varepsilon}_D$) by the diffusion accommodated process

$$\dot{\varepsilon}_D = 100\frac{\Omega}{kTd^2}\left(\sigma - \frac{0.72\Gamma}{d}\right)D_L\left(1 + \frac{3.3\delta}{d}\frac{D_{gb}}{D_L}\right) \quad (2)$$

where Ω is the atomic volume, d is the grain size, Γ is the grain-boundary free energy, D_L is the lattice diffusion coefficient, D_{gb} is the grain-boundary diffusion coefficient, δ is the thickness of the grain boundary, and k is Boltzmann's constant. The equation is similar to the sum of classical lattice diffusion creep (Nabarro–Herring creep [20, 21]) and the grain-boundary diffusion creep (Coble creep [22]) if the threshold stress, $0.72\Gamma/d$, is neglected and the factor of 100 is replaced by a factor of 14.

A basic assumption of diffusion-accommodated GBS (Equation 2) is that the grain-boundary surface is a perfect sink or source for vacancies. If this assumption is not satisfied, the diffusion creep is controlled by the interface reaction [23–28]. The effect of interface reaction can be observed as stress exponents larger than 1 (non-Newtonian flow) or as the existence of threshold stress (Bingham-type creep). Several constitutive equations for the interface-reaction controlled diffusion creep have been proposed, based on some specific models of grain-boundary structure. For example, when the dislocation-like line defects at grain boundaries are assumed to be the sink and source of vacancies, the strain rate ($\dot{\varepsilon}_i$) is given by [19, 23, 25, 26, 28]

$$\dot{\varepsilon}_i = B\frac{\sigma^2}{d} \quad (3)$$

where B is a coefficient. When the interface-reaction controlled GBS and the diffusion-accommodated GBS are sequential processes, the strain rate is expressed by the following equation

$$\frac{1}{\dot{\varepsilon}} = \frac{1}{\dot{\varepsilon}_D} + \frac{1}{\dot{\varepsilon}_i} \quad (4)$$

The dominant deformation mechanism of 2 mol %

0022–2461/91 $03.00 + .12

Y_2O_3-stabilized TZP was dependent on grain size; the value of stress exponent, 2, approached unity, with the coarsening of grain size by heat-treatment. This behaviour could be simulated fairly well by Equation 4 where $\dot{\varepsilon}_D$ was expressed as follows, instead of as Equation 2 [29]

$$\dot{\varepsilon}_D = A' \frac{\sigma}{d^2} \quad (5)$$

where A' is a coefficient.

According to this model, the superplasticity of fine-grained Y-TZP was related to GBS accommodated by the interface-reaction controlled diffusion, while the deformation of materials made of coarser grains was related to diffusion creep. The stress exponents reported for some cubic ZrO_2 polycrystals with higher Y_2O_3 concentration were intermediate between 1 and 2 [8–12]. In these cases, the contribution of diffusion-controlled creep and that of interface-reaction controlled creep can be separated using Equation 4. Thus, this procedure can serve to investigate the diffusion coefficient of cations and the interface-reaction rate as a function of solute concentration in ZrO_2.

The present work was undertaken to study the deformation in various ZrO_2 polycrystals having different grain sizes, solute species, and solute concentrations, so that the effect of solute ion on diffusion coefficient of cations and that on interface reaction have been investigated.

2. Experimental procedure

2.1. Specimen preparation

All materials used for this study were fabricated by sintering coprecipitated ZrO_2 powders (Tosoh Co., Japan) containing rare-earth oxides in solid solution [30–33]; 2 mol % Y_2O_3 (2Y), 3 mol % Y_2O_3 (3Y), 4 mol % Y_2O_3 (4Y), 6 mol % Y_2O_3 (6Y), 8 mol % Y_2O_3 (8Y), and 12 mol % CeO_2 (12Ce). Properties of the materials are shown in Table I. The densities of all specimens were determined by Archimedes' technique. The microstructure of as-received materials was observed by scanning electron microscope (SEM) on the polished and thermally etched surfaces. The studied materials were composed of equiaxed grains. The average grain size (d) was defined as $d = 1.78L$, where L was the average linear intercept length. The ZrO_2 grains are either tetragonal (t-ZrO_2) or cubic (c-ZrO_2) depending on respective compositions according to the phase diagrams of the ZrO_2–Y_2O_3 and ZrO_2–CeO_2 systems in the temperature range 1150 to 1500 °C.

TABLE I Properties of ZrO_2 polycrystals adopted for experiments

Material	Composition (mol %)	Density ($g\,cm^{-3}$)	Grain size (μm)	Phase
2Y	2 Y_2O_3	6.04	0.55	t
3Y	3 Y_2O_3	6.07	0.51	t + c
4Y	4 Y_2O_3	6.03	0.75	t + c
6Y	6 Y_2O_3	5.95	5.5	c + t
8Y	8 Y_2O_3	5.92	14	c
12Ce	12 CeO_2	6.22	1.9	t

t, tetragonal; c, cubic.

Specimens for tension and tensile creep tests were diamond-machined from sintered plates (20 mm × 80 mm × 4 mm). Tension specimens had a gauge length of 30 mm with a circular cross-section of about 3 mm diameter. Specimens used in tensile creep tests were designed to have "targets" on both sides of the gauge length portion (3 mm × 20 mm) so that the creep strain could be measured.

2.2. Tensile creep test

Tensile creep tests at constant loads were performed in air by using an apparatus with an electro-optical extensometer. At the testing temperature, the applied load for one specimen was sequentially increased whenever the elongation at one load reached nominal strain of 0.5% or that of 1%. Stress exponents were obtained by stress and strain rate which were calculated from the creep curves.

For measurement of activation energy, the tests were conducted at a constant load corresponding to a nominal stress of 20 MPa. The temperature was sequentially elevated whenever the elongation at one temperature reached nominal strain of 0.5% or that of 1%.

2.3. Tension test

Tension tests at constant cross-head speeds were conducted in air using a universal testing machine. Displacement of the cross-head was measured and calibrated to the elongation against the gauge-length portion of the specimen. True stress–true strain curves were obtained from load–elongation curves by assuming a uniform deformation. Prior to the tests, some specimens (2Y, 3Y, 4Y) were heat-treated to alter the grain size. The stress exponent was obtained by changing the cross-head speed rapidly during the test.

3. Results

3.1. Creep curve

The creep curve for 2Y at 1250 °C is shown in Fig. 1. The creep curve exhibited a transient state with de-

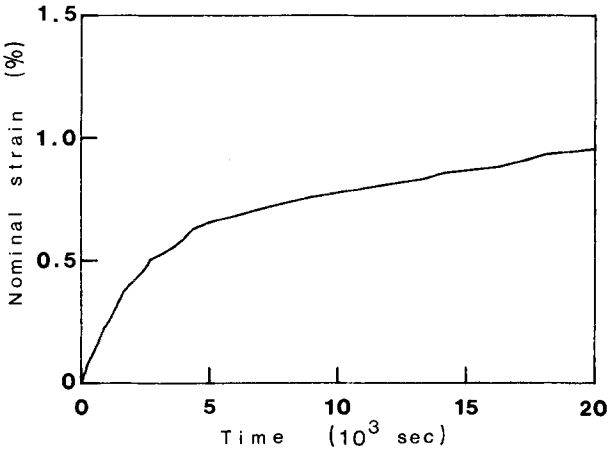

Figure 1 Creep curve for 2 mol % Y_2O_3-stabilized tetragonal ZrO_2 polycrystals (2Y), at 1250 °C and 2.6 MPa.

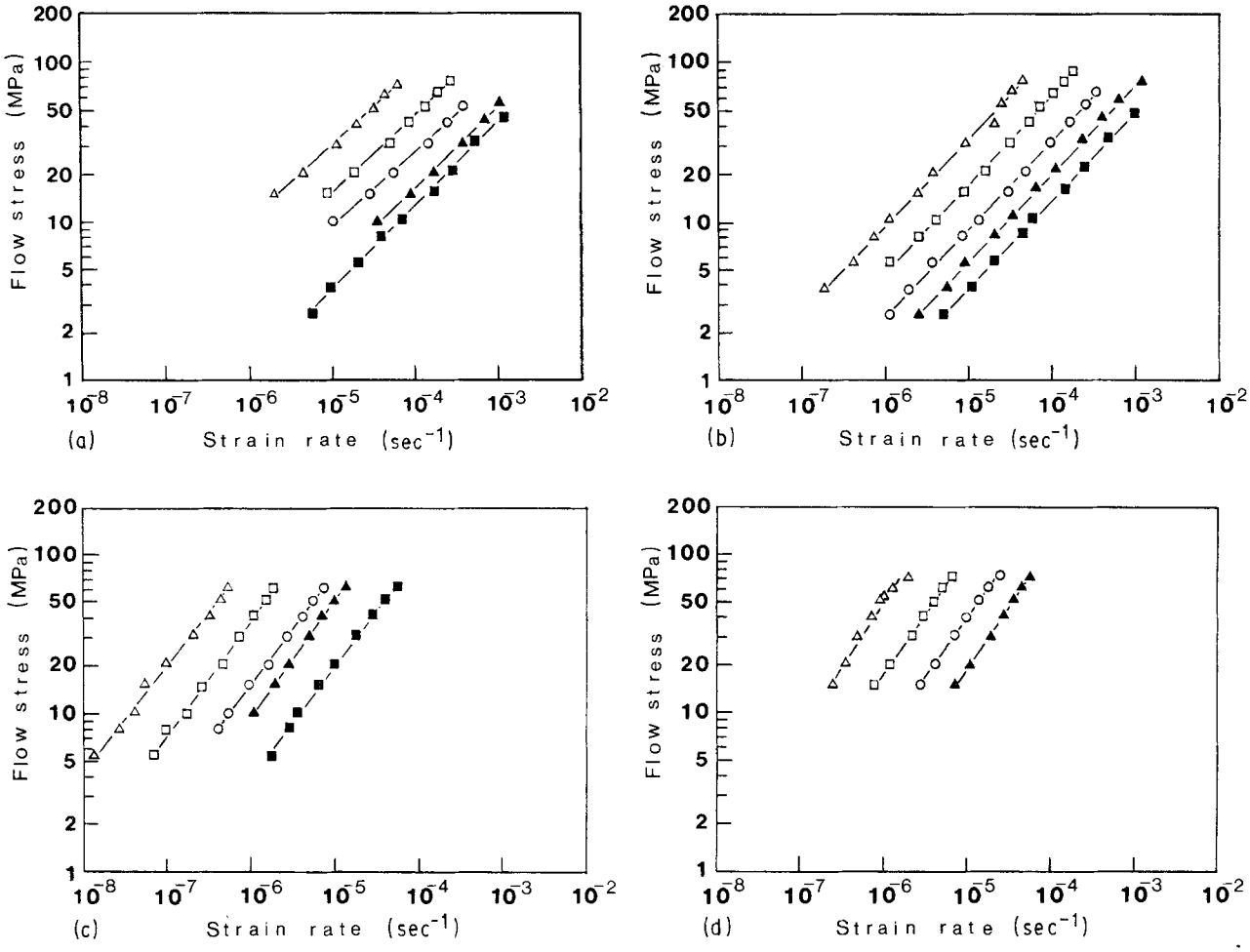

Figure 2 Log stress–log strain rate curves for (a) 3 mol % Y_2O_3-stabilized ZrO_2 polycrystals (3Y), (△) 1250 °C, n = 2.1, (□) 1300 °C, n = 2.1, (○) 1350 °C, n = 2.2, (▲) 1400 °C, n = 2.0, (■) 1450 °C, n = 1.9; (b) 4 mol % Y_2O_3-stabilized ZrO_2 polycrystals (4Y), n = 1.8, (△) 1250 °C, (○) 1350 °C, (□)1300 °C, (▲)1400 °C, (■) 1450 °C; (c) 6 mol % Y_2O_3-stabilized ZrO_2 polycrystals (6Y), (△) 1250 °C, n = 1.5, (□) 1300 °C, n = 1.4, (○) 1350 °C, n = 1.4, (▲) 1400 °C, n = 1.4, (■) 1450 °C, n = 1.4; (d) 12 mol % CeO_2-stabilized ZrO_2 polycrystals (12Ce), (△) 1250 °C, n = 1.2, (□) 1300 °C, n = 1.3, (○) 1350 °C, n = 1.3, (▲) 1400 °C, n = 1.3.

creasing creep rate and a steady state at strains beyond 0.8%. The duration of the transient state increased with decreasing temperature and stress level. This anelastic behaviour may cause an error in determining stress exponents in a range of low strain rates (less than $10^{-6}\,sec^{-1}$) when using a stress change method during the creep test. For example, the stress relaxation test sometimes caused spurious threshold stress, or the stress increasing test gave somewhat smaller stress exponents. In order to avoid ambiguities, further analysis in this work was conducted only on the steady creep rates.

3.2. Stress exponent

The relationship between stress and strain rate which was obtained by tensile creep tests is shown with logarithmic scales for 3Y, 4Y, 6Y, and 12Ce in Fig. 2a to d, respectively. The data for 2Y were described elsewhere. The constant value of stress exponent for each material was obtained in the temperature range 1250 to 1450 °C. We observed [29] a decrease in stress exponent of 2Y from a value of 2 to a value of about 1 on increasing the grain size by heat treatment. A similar phenomenon was also observed for 3Y and 4Y in the tension tests. The relationship between stress exponent and grain size is illustrated in Fig. 3. For all the materials, the values of stress exponent were intermediate between 2 and 1, and reduced with increasing grain size.

3.3. Activation energy

The temperature dependence of creep rate is plotted in Fig. 4. The data for 3Y are not shown in Fig. 4 for the

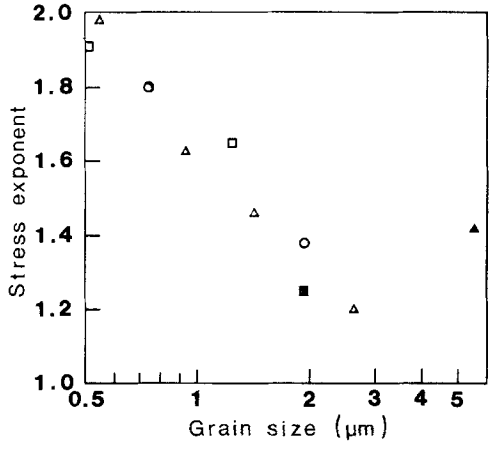

Figure 3 Variation of stress exponent with grain size. (△) 2Y, (□) 3Y, (○) 4Y, (▲) 6Y, (■) 12Ce.

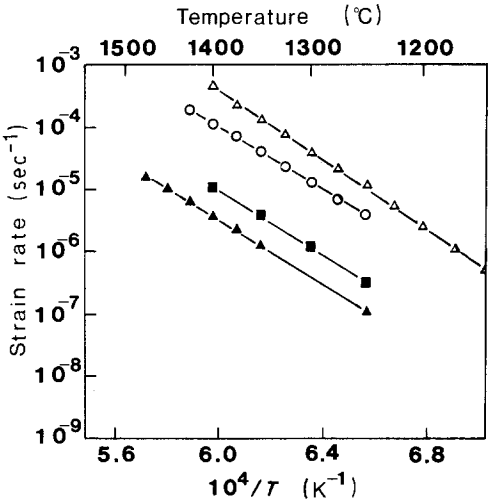

Figure 4 Comparison of log strain rate–reciprocal absolute temperature curves for various ZrO_2 polycrystals. 20 MPa; Q_{app} (kJ mol^{-1}) = (△) 533 for 2Y, (○) 480 for 4Y, (▲) 491 for 6Y, and (■) 498 for 12Ce.

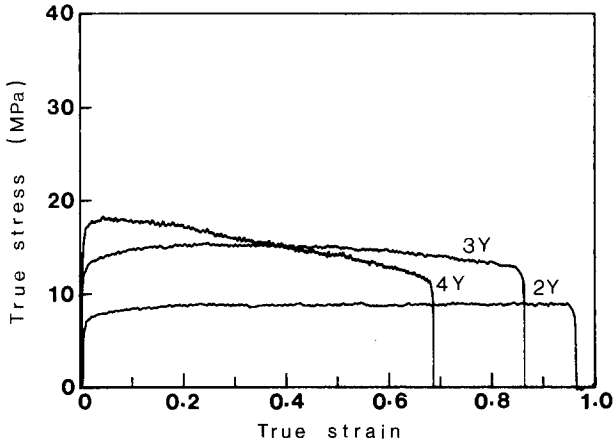

Figure 5 Comparison of true stress–true strain curves for various Y_2O_3-stabilized ZrO_2 polycrystals, at 1450 °C and strain rate = 2.70×10^{-4} sec^{-1}.

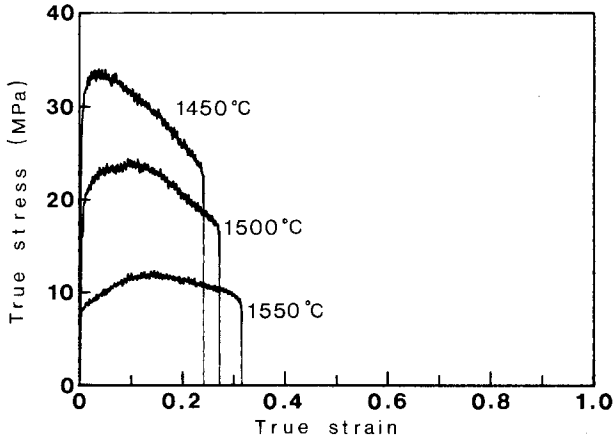

Figure 6 True stress–true strain curves for 12 mol % CeO_2-stabilized ZrO_2 polycrystals; strain rate = 6.94×10^{-5} sec^{-1}.

sake of clarity, because these are almost identical to the data for 4Y. The apparent activation energy was calculated assuming Equation 1 holds. The apparent activation energy of 2Y, 4Y, and 6Y were 533, 480, and 491 kJ mol^{-1}, respectively. The strain rates of 12Ce at 20 MPa were read from Fig. 2d and plotted in Fig. 4. The apparent activation energy of 12Ce was 498 kJ mol^{-1}. For the materials 2Y, 4Y, and 6Y, a similar calculation from the strain rates read from Fig. 2 yielded apparent activation energies of 504, 428, and 486 kJ mol^{-1}, respectively. The apparent activation energy of the deformation was far larger than that of oxygen diffusion [2, 3] and seemed to be related to cation diffusion [4, 5].

Although the deformation mechanism of materials with a stress exponent of about 2 (2Y and 4Y) was clearly different from that of materials with a stress exponent of about 1 (6Y and 12Ce), the activation energies of both material groups were approximately the same. Furthermore, the difference in crystalline phase did not affect the apparent activation energy of the materials with a stress exponent of about 1, because the activation energy of 6Y, which was almost completely cubic, was very close to that of 12Ce, which was tetragonal.

3.4. Stress–strain curve

The true stress–true strain curves of tension tests at a constant cross-head speed are shown in Fig. 5. The flow curves for the fine-grained materials with a stress exponent of about 2 (2Y, 3Y and 4Y), showed superplastic elongations. The flow stress was lowered by decreasing the solute concentration, and the elongation to failure increased with decreasing flow stress. When the tension test of the materials with a stress exponent of about 1 (6Y and 12Ce) was conducted under the same experimental conditions as described in Fig. 5, instantaneous fracture was observed with no deformation. Fig. 6 shows the stress–strain curves of 12Ce elongated at a lower strain rate. Although the elongation to failure increased with elevating temperature (nominal strain of 34% was obtained at 1550 °C), superplastic elongation could not be achieved for 12Ce.

4. Discussion

4.1. Effect of solute ions on the lattice diffusion coefficient

In this section we postulate that the deformation of ZrO_2 polycrystals involves the diffusion creep controlled by interface reaction (Equation 3) and the creep controlled by cation lattice diffusion (Equation 5). The total strain rate is supposed to be expressed by Equation 4.

When the stress exponent of ZrO_2 polycrystals was intermediate between 1 and 2, the coefficient of interface reaction (B) in Equation 3 and the coefficient (A') in Equation 5 were determined by parameter fitting. The lattice diffusion coefficient of cations was calculated from the coefficient (A') by assuming that the Equation 5 coincided with the Nabarro–Herring creep which was given by

$$\dot{\varepsilon}_{N-H} = \frac{14\Omega D_L}{kT}\frac{\sigma}{d^2} \quad (6)$$

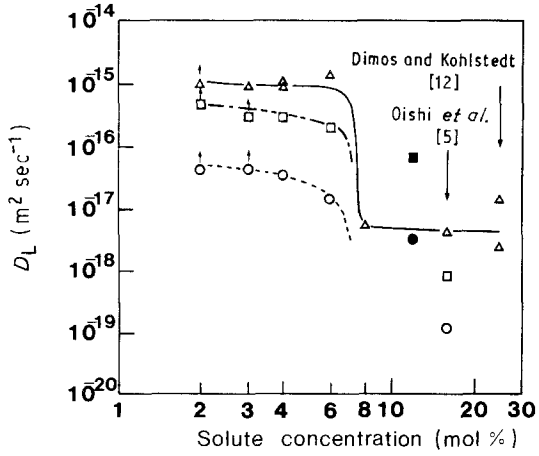

Figure 7 Relationship between lattice diffusion coefficient and solute concentration. (△, □, ○) Y_2O_3, (■, ●) CeO_2; (△) 1450 °C, (□, ■) 1350 °C, (○, ●) 1250 °C.

where Ω is the molecular volume of ZrO_2. When the stress exponent was 2, the coefficient of A' was arbitrary, and only the lower bounds of A' could be determined.

The relationship between lattice diffusion coefficient and solute ion concentration is plotted in Fig. 7. The data points for 16 mol % Y_2O_3 were the Zr–Hf lattice interdiffusion coefficient obtained by Oishi *et al.* [5]. Dimos and Kohlstedt [12] observed the Nabarro–Herring creep of 25 mol % Y_2O_3-stabilized ZrO_2 with average grain sizes between 2.5 and 14.5 μm. The data points for 25 mol % Y_2O_3 were calculated from their results. A great difference in lattice diffusion coefficient existed at the critical concentration of 6 mol % Y_2O_3. While the lattice diffusion coefficients at 1450 °C are 10^{-15} m^2 sec^{-1} for materials containing less than 6 mol % Y_2O_3, these decreased to a value of about 10^{-17} m^2 sec^{-1} for materials containing more than 8 mol % Y_2O_3. A similar variation of diffusion coefficient was also noted at 1350 and 1250 °C.

The diffusion coefficient is expressed as follows

$$D = [X]D_x \tag{7}$$

where D is the self-diffusion coefficient of the rate-controlling ion, $[X]$ is the concentration of the rate-controlling defect and D_x is the diffusion coefficient of the defect. The diffusion coefficient will vary with the solute concentration, because the concentration of defects is a function of solute concentration. Considering simple point defect chemistry, the concentration of oxygen vacancies $[V_O^{\cdot\cdot}]$, the majority defect, is given by

$$[V_O^{\cdot\cdot}] \propto c^{1/3} \tag{8}$$

where c is the concentration of Y_2O_3. The concentration of cation vacancies $[V_{Zr}^{4'}]$, and that of the interstitial $[Zr^{4\cdot}]$, are given by [34]

$$[V_{Zr}^{4'}] \propto c^{-2/3} \tag{9}$$

$$[Zr^{4\cdot}] \propto c^{2/3} \tag{10}$$

The slope at concentrations from 2 to 6 mol % Y_2O_3 in Fig. 7 took negative values. However, the variation of diffusion coefficient at concentrations larger than 8 mol % Y_2O_3 cannot be explained by this simple point defect chemistry.

St-Jacque and Angers [11] also observed the effect of solute concentration on creep rate of CaO-stabilized ZrO_2. They explained the decrease in creep rate of CaO-stabilized ZrO_2 (> 15 mol % CaO) by variation of the frequency factor of diffusion coefficient. According to their discussions, the decrease in the frequency factor occurred due to the relaxation of the lattice which was caused by the increase of oxygen vacancies. Our results on Y_2O_3-stabilized ZrO_2 indicated that the small change at the critical concentration (from 6 to 8 mol % Y_2O_3) produced a great difference in the diffusion coefficient. Thus it seems that some factors besides the concentration of oxygen vacancies are also responsible for the phenomenon. A similar anomaly in the relation between ionic transport process and solute concentration has also been found in conductivity which involves oxygen vacancies [1]. The variation of conductivity exhibits a maximum around 12 to 13 mol % in CaO-stabilized ZrO_2 and around 8 to 9 mol % in Y_2O_3-stabilized ZrO_2. The reason why the variation of anion diffusion with concentration of solute ion has some correlation with the variation of cation diffusion, is not clear yet. However, we feel that a unified theory to explain the diffusion of both anions and cations should be developed by incorporating the interaction between vacancies.

When ZrO_2 is doped with CeO_2, the concentration of oxygen vacancies is not dependent on the concentration of CeO_2. If we assume that the diffusion of cations is affected by the interaction between cation and anion vacancies, the drastic variation in lattice diffusion coefficient with solute concentration will not be observed in the ZrO_2–CeO_2 system. The diffusion coefficient of cations in 12 mol % CeO_2-stabilized ZrO_2, which had a low concentration of oxygen vacancies, was close to the values for materials with low concentrations of Y_2O_3 solution (Fig. 7). This is in agreement with the fact reported by Oishi *et al.* [5] that the self-diffusion coefficient of zirconium was not sensitive to doped cations.

4.2. Role of grain-boundary diffusion on creep

The apparent grain-boundary diffusivities (δD_{gb}) of ZrO_2 polycrystals were calculated by assuming that the deformation could be described by the equation for Coble creep.

$$\dot{\varepsilon}_{Coble} = \frac{14\pi\sigma\Omega\delta D_{gb}}{kTd^3} \tag{11}$$

The apparent grain-boundary diffusivities for various ZrO_2 polycrystals were plotted against the grain size, as shown in Fig. 8. The solid line in Fig. 8 indicates the grain-boundary diffusivity of the cation which was measured by the tracer diffusion experiments [5]. There was a fairly good agreement in the value of apparent grain-boundary diffusivity between the creep data (4Y and 6Y) and the tracer diffusion data. However, the apparent grain-boundary diffusivity obtained

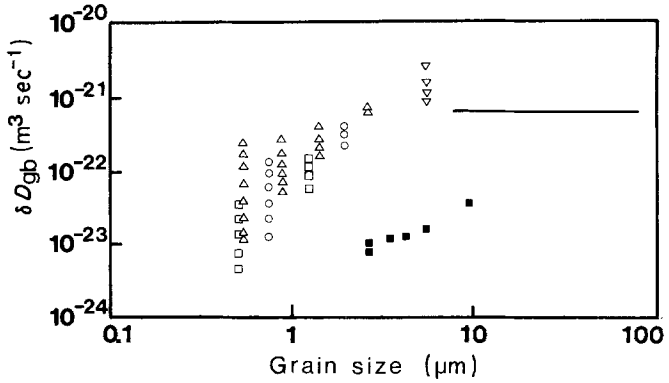

Figure 8 Relationship between apparent grain-boundary diffusivity and grain size at 1450 °C. Material: (△) 2Y, (□) 3Y, (○) 4Y, (▽) 6Y, (■) 25Y [12].

using the creep data was not a constant, and it increased with increasing grain size.

When the amorphous film exists at grain boundaries of ZrO_2 polycrystals, the width of the grain boundary can be regarded as approximately the same as that of the amorphous film. If the volume fraction of the amorphous phase is invariable, the thickness of the grain boundary increases with coarsening of the grain size

$$\delta = \delta_0 d/d_0 \tag{12}$$

where d_0 is the initial grain size and δ_0 is the initial thickness of the grain boundary. The apparent grain-boundary diffusivity ($\delta_0 D_{gb} d/d_0$) increases with grain size. Consequently, even the constitutive equation of grain-boundary diffusion creep can be expressed by Equation 5. In this case, the apparent grain-boundary diffusivity is not affected by the solute concentration in ZrO_2, but by the amount of amorphous phase and by its composition.

4.3. Effect of solute ions on the interface reaction

Fig. 9 shows that the coefficient (B) of interface reaction in Equation 3 varies with solute concentration. The data points for 25 mol % Y_2O_3 were calculated from the results of Dimos and Kohlstedt [12]. When these data are compared with the results obtained for 2Y, 3Y, 4Y and 6Y, the interface-reaction rate seems to decrease with increasing solute concentration. The interface-reaction rate, however, cannot be described by a simple function of solute concentration, because there is an anomaly at 3 mol % Y_2O_3.

Arzt *et al.* [28] developed an atomistic model for interface reaction by considering the mobility of grain-boundary dislocations which were a source and a sink of vacancies. It should be noted that their model for solute-drag-limited diffusional creep predicts the following rate equation

$$\dot{\varepsilon} = \frac{B_1 \Omega \sigma^2 D_s}{TC_0 d} \tag{13}$$

where D_s is the diffusion coefficient for the solute, C_0 is the solute concentration and B_1 is a coefficient. In their model, the activation energy was related to solute diffusion in the lattice rather than to boundary diffusion, and the interface-reaction rate was inversely proportional to solute concentration. Equation 13 is not inconsistent with our results on interface reaction of ZrO_2. However, it is known that there is a thin amorphous film at grain boundaries of ZrO_2 polycrystals [35, 36]. Thus the role of grain-boundary dislocation is not fully understood for these materials. Although some recent investigations suggested that the amorphous film at two-grain junctions in oxides [37, 38] or non-oxides [39] had some structure, our knowledge of the grain-boundary structure in such a system is not sufficient to build an atomistic model for the interface reaction. We believe that studies of deformation can provide insight into the structure and dynamics at grain boundaries having amorphous films.

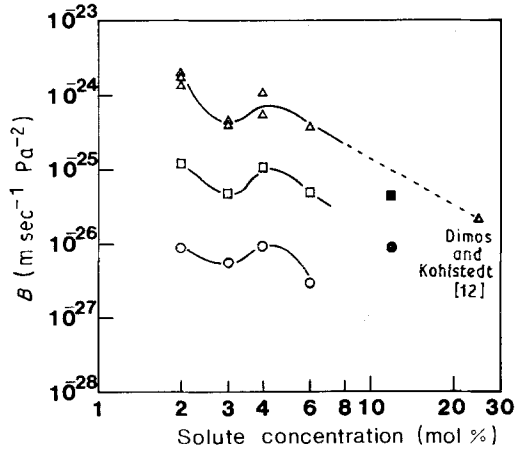

Figure 9 Relationship between interface-reaction rate and solute concentration. (△, □, ○) Y_2O_3, (■, ●) CeO_2; (△) 1450 °C, (□, ■) 1350 °C, (○, ●) 1250 °C.

5. Conclusion

A model for deformation of ZrO_2 in which both diffusion and interface reaction acted sequentially during grain-boundary sliding has been proposed to explain the variation of stress exponent with grain size in the creep of ZrO_2 doped with 2 mol % Y_2O_3. This model has been successfully applied to describe the deformation of ZrO_2 polycrystals containing 3 to 8 mol % Y_2O_3 or 12 mol % CeO_2. According to this model, the mechanism of superplasticity is the grain-boundary sliding accommodated by the interface-reaction controlled diffusion. When the grain size is relatively large and the lattice diffusion is slow, Newtonian flow controlled by either diffusion or grain-boundary diffusion is observed. When the grain

size is small and the diffusion is fast, non-Newtonian flow controlled by interface reaction could be observed. Both the lattice-diffusion coefficient of cations and the interface-reaction rate are affected by the concentration of solute ions.

Acknowledgement

The authors thank Dr Kiyoshi Hayakawa for his helpful discussions.

References

1. J. F. BAUMARD and P. ABELAND, in "Advances in Ceramics", Vol. 12, edited by N. Claussen, M. Rühle and A. H. Heuer (American Ceramic Society, Columbus, Ohio, 1984) p. 555.
2. W. D. KINGERY, J. PAPPIS, M. E. DOTY and D. C. HILL, *J. Amer. Ceram. Soc.* **42** (1959) 393.
3. L. A. SIMPSON and R. E. CARTER, *ibid.* **49** (1966) 139.
4. W. H. RHODES and R. E. CARTER, *ibid.* **49** (1966) 244.
5. Y. OISHI, K. ANDO and Y. SAKKA, in "Advances in Ceramics", Vol. 7, edited by M. F. Yan and A. H. Heuer (American Ceramic Society, Columbus, Ohio, 1983) p. 208.
6. N. BONANOS, R. K. SLOTWINSKI, B. C. H. STEELE and E. P. BUTLER, *J. Mater. Sci. Lett.* **3** (1984) 245.
7. S. P. S. BADWAL, *ibid.* **6** (1987) 1419.
8. P. E. EVANS, *J. Amer. Ceram. Soc.* **53** (1970) 365.
9. M. S. SELTZER and P. K. TALTY, *ibid.* **58** (1975) 124.
10. R. G. ST-JACQUES and R. ANGERS, *ibid.* **55** (1972) 571.
11. *Idem., Trans. Brit. Ceram. Soc.* **72** (1973) 285.
12. D. DIMOS and D. L. KOHLSTEDT, *J. Amer. Ceram. Soc.* **70** (1987) 531.
13. F. WAKAI, S. SAKAGUCHI and Y. MATSUNO, *Adv. Ceram. Mater.* **1** (1986) 259.
14. F. WAKAI, S. SAKAGUCHI and H. KATO, *Yogyo-Kyokai-Shi* **94** (1986) 721.
15. F. WAKAI, N. MURAYAMA, S. SAKAGUCHI, H. KATO and K. KURODA, "Advances in Ceramics", Vol. 24, "Science and Technology of Zirconia III", edited by S. Somiya, N. Yamamoto and H. Yanagida (American Ceramic Society, Columbus, Ohio, 1988) p. 583.
16. C. CARRY and A. MOCELLIN, *Ceram. Int.* **13** (1987) 89.
17. R. DUCLOS and J. CRAMPON, *J. Mater. Sci. Lett.* **6** (1987) 905.
18. F. WAKAI and H. KATO, *Adv. Ceram. Mater.* **3** (1988) 71.
19. M. F. ASHBY and R. A. VERRALL, *Acta Metall.* **21** (1973) 149.
20. F. R. N. NABARRO, *Phil. Mag.* **16** (1967) 231.
21. C. HERRING, *J. Appl. Phys.* **21** (1950) 437.
22. R. L. COBLE, *ibid.* **34** (1963) 1679.
23. M. F. ASHBY, *Scripta Metall.* **3** (1969) 837.
24. G. W. GREENWOOD, *ibid.* **4** (1970) 171.
25. B. BURTON, *Mater. Sci. Engng* **10** (1972) 9.
26. *Idem., Phil. Mag. A* **48** (1983) L9.
27. R. M. CANNON, W. H. RHODES and A. H. HEUER, *J. Amer. Ceram. Soc.* **63** (1980) 46.
28. E. ARZT, M. F. ASHBY and R. A. VERRAL, *Acta Metall.* **31** (1983) 1977.
29. F. WAKAI and T. NAGANO, *J. Mater. Sci. Lett.* **7** (1988) 607.
30. T. K. GUPTA, J. H. BECHTOLD, R. C. KUZNICKI and L. H. CADOFF, *J. Mater. Sci.* **12** (1977) 2421.
31. F. F. LANGE, *ibid.* **17** (1982) 240.
32. K. TSUKUMA, Y. KUBOTA and T. TSUKIDATE, in "Advances in Ceramics", Vol. 12, edited by N. Claussen, M. Rühle and A. H. Heuer (American Ceramic Society, Columbus, Ohio, 1984) p. 382.
33. K. TSUKUMA and M. SHIMADA, *J. Mater. Sci.* **20** (1985) 1178.
34. A. DOMINGUEZ-RODRIGUEZ, V. LANTERI and A. H. HEUER, *J. Amer. Ceram. Soc.* **69** (1986) 281.
35. M. RÜHLE, N. CLAUSSEN and A. H. HEUER (eds) in "Advances in Ceramics", Vol. 12 (American Ceramic Society, Columbus, Ohio, 1984) p. 352.
36. M. L. MECARTNEY, *J. Amer. Ceram. Soc.* **70** (1987) 54.
37. D. R. CLARK, *ibid.* **70** (1987) 15.
38. J. E. MARION, C. H. HSUEH and A. G. EVANS, *ibid.* **70** (1987) 708.
39. Y. IKUHARA, H. KURISHITA and H. YOSHINAGA, *Yogyo-Kyokai-Shi* **95** (1987) 638.

Received 8 April
and accepted 7 September 1988